
Effective shear viscosity and dynamics of suspensions of micro-swimmers from small to moderate concentrations

V. Gyrya · K. Lipnikov · I. Aranson · L. Berlyand

Received: date / Accepted: date

Abstract Recently, there has been a number of experimental studies convincingly demonstrating that a suspension of self-propelled bacteria (microswimmers in general) may have an effective viscosity significantly smaller than the viscosity of the ambient fluid. This is in sharp contrast with suspensions of hard passive inclusions, whose presence always increases the viscosity. Here we present a 2D model for a suspension of microswimmers in a fluid and analyze it analytically in the dilute regime (no swimmer-swimmer interactions) and numerically using a Mimetic Finite Difference discretization. Our analysis shows that in the dilute regime (in the absence of rotational diffusion) the effective shear viscosity is not affected by self-propulsion. But at the moderate concentrations (due to swimmer-swimmer interactions) the effective viscosity decreases linearly as a function of the propulsion strength of the swimmers. These findings prove that *(i)* a physically observable decrease of viscosity for a suspension of self-propelled microswimmers can be explained purely by hydrodynamic interactions and *(ii)* self-propulsion and interaction of swimmers are both essential to the reduction of the effective shear viscosity.

We also performed a number of numerical experiments analyzing the dynamics of swimmers resulting from pairwise interactions. The numerical results agree with the physically observed phenomena (e.g., attraction of swimmer to swimmer and swimmer to the wall). This is viewed as an additional validation of the model and the numerical scheme.

V. Gyrya
The Pennsylvania State University, Department of Mathematics, University Park, PA, 16802,
USA, E-mail: gyrya@math.psu.edu

K. Lipnikov
Los Alamos National Laboratory, MS B284, Los Alamos, NM 87545, USA

I. Aranson
Argonne National Laboratory, Division of Material Science, Argonne, IL, USA

L. Berlyand
The Pennsylvania State University, Department of Mathematics, University Park, PA, 16802,
USA

1 Introduction

In recent years there have been a number of experimental studies convincingly demonstrating that self-propulsion can significantly change the rheological properties of suspensions.

In [1] it was shown that self-propelled bacteria (*Escherichia coli*; $1\mu\text{m}$ wide and $2\text{--}3\mu\text{m}$ long; concentration around 10% by volume) enhanced the diffusion of tracer particles ($1\text{--}10\mu\text{m}$ in size) by 2–3 orders of magnitude in the quasi-two-dimensional setting of a freely suspended soap film. Further analysis of this enhanced diffusion in the flow created by self-propelled microswimmers (*Chlamydomonas reinhardtii*) was performed recently in [2]. In [3,4] it was demonstrated that self-propelled bacteria (*Bacillus subtilis*; $.7\mu\text{m}$ wide and $5\mu\text{m}$ long; concentration around 3% – 5% by volume) could reduce the viscosity of the suspension by up to five times when compared to passive/dormant bacteria. The experiments were also performed in a thin film. The activity of the bacteria was controlled by changing the supply of oxygen.

The above experiments demonstrate that suspensions of active swimmers may have drastically different properties than suspensions of passive inclusions. Exploiting these properties may lead to new or improved engineering solutions (e.g., self-replicating micromixers). Explaining and quantifying the changing viscosity for a suspension of microswimmers is the goal of this paper. We identify the following key features affecting this viscosity and the difficulties related to modeling and analysis of microswimmers: (i) inhomogeneity of the fluid due to inclusions, (ii) elongated shape of the inclusions, (iii) particle-particle interactions, and the new feature – (iv) self-propulsion.

The rheological properties of passive suspensions have been studied extensively for over a century. The analysis of the effective viscosity for passive suspensions dates back to the famous work of Einstein [5], where he computed the linear (in volume fraction ϕ) correction to the viscosity for a suspension of neutrally buoyant inert hard spheres in a Newtonian fluid in the dilute limit ($\phi \rightarrow 0$). Jeffery [6] extended the analysis from spherical to ellipsoidal inclusions, where he demonstrated the dependence of the viscosity on the distribution of orientations of the inclusions. Hinch and Leal [7,8] analyzed the limiting distribution of orientations of ellipsoids in a shear flow in the presence of a rotational Brownian motion and used this to obtain the effective viscosity for a suspension of ellipsoids. Batchelor and Green [9] were the first to consider pairwise particle interactions in order to find the $O(\phi^2)$ correction to Einstein’s result [5]. Up to this point, all works have involved formal asymptotics.

In the 1980s, rigorous homogenization results were first obtained for moderate concentrations of particles by Levy and Sanchez-Palencia in [10] and Nunan and Keller in [11] for periodic distributions of inclusions. Results for the densely-packed regime were more recently proven in [12–14].

Some of the earlier works in modeling the swimming at low Reynolds number were done by Taylor [15], who studied self-propulsion of a waving sheet, and Purcell [16], who studied the basics of self-propulsion of microswimmers. The modeling of swimmers can be divided into two categories based on whether they change their shape or not. Examples of models of swimmers changing their shape are a three-linked sphere swimmer [17,18] and a swimmers with rotating tail [19]. These models are attractive because the real-world swimmers (bacteria, fish, etc.) swim due to shape changes (rotation of flagella, waving of the tail, etc.). Unfortunately, the analysis of these models is difficult and we are not aware of a rheological analysis being done for

suspensions of such swimmers, although the dynamics of such swimmers due to their interaction was analyzed in a number of papers (e.g., [19,20]).

The other category of models are those where the swimmers do not change shape. The propulsion here is either due to a prescribed effective force or an effective relative velocity of the fluid on a part of the surface of the swimmer. Self-propulsion is enforced by equating to zero the total force and torque on each of the swimmers.

Ishikawa and Pedley [21], modeling microswimmers as spheres with a prescribed relative velocity on the surface of the spheres, observed a decrease in viscosity only for swimmers with shifted center of gravity in the presence of a gravitational field. In [21] the results are obtained using boundary integral methods. Shelley and Saintillan [22] modeled swimmers as slender rods with tangential traction prescribed on a part of the boundary, for which they observed behavior reminiscent of that in the physical experiment for *Bacillus subtilis* [23–25]. In particular, they observed local nematic ordering of rod-like swimmers that had a significant impact on their mean swimming speed.

In [26] authors consider a phenomenological model of active gels, treating them from the perspective of liquid crystals. In particular, they are interested in the effective viscosity of active gels near “nematic” phase. They view suspension of microswimmers as one of examples of active gels. In our view, attainability of the “nematic” phase understood as an almost perfect ordering in suspensions of microswimmers is debatable. On the other hand, the “nematic” phase may be feasible for suspensions of engineered microswimmers that swim due to externally applied alternating magnetic field (e.g. [27]) and, therefore, could be synchronized to swim in the same direction.

Another notable work presenting phenomenological arguments relating the viscosity of suspensions to the activity of particles is [28]. In [28], a tensor order parameter Q is used to characterize the local ordering of the system (i.e., the alignment of swimming particles to each other). The governing dynamics for Q is borrowed from the theory of systems with nematic ordering and is phenomenological. In particular, the relationship of the evolution of the order parameter to the microscopic alignment dynamics has not been clarified, and the very possibility of arriving at macroscopic expressions for the effective viscosity from first-principle arguments has not been established. In this work, we begin to fill this gap by proposing a model that allows for an analytic and numerical analysis of the dynamics and ultimately explains the observed effects of decreasing viscosity.

In the recent work [29] Haines, Aranson, Berlyand and Karpeev observed a decrease of the effective viscosity in the *dilute limit* (no swimmer-swimmer interactions) for slightly elongated disks with self-propulsion resulting from a point force in the fluid (attached to the body). They considered two types of background flow: extensional and oscillatory shear flows. In both cases, the decrease of viscosity was attributed to swimmers aligning with the flow, supporting the background flow. In [30] a three-dimensional model was considered which is an extension of [29] with addition of the Brownian rotational noise designed to model tumbling of bacteria. The analytic formula for the effective viscosity was obtained in the dilute limit for shear and straining background flows. The key feature for the shear flow responsible for the reduction of viscosity here is the Brownian rotational noise.

In this paper, we present a two-dimensional mathematical model of the swimmer-fluid system. The elongated body of the swimmer is modeled by an ellipse. The “front” half of the ellipse represents the solid surface and the “back” half represents the surface

covered with flagella or cilia (e.g. *Paramecium*) that exert the propulsion force onto the fluid.

We consider both dilute and moderate concentration regimes. In the dilute regime (no swimmer-swimmer interactions) we demonstrate analytically that self-propulsion has no effect on the effective viscosity. Therefore, we show that the elongated shape of the swimmers and the propulsion force are not sufficient to change the effective viscosity as compared to the passive suspensions.

On the other hand, the numerical analysis of the moderate concentration regime, taking into account all interactions, showed a decrease of the effective viscosity with propulsion strength of the swimmers. At this concentration regime all of the above features (*ii-iv*) are present: the elongated shape of the swimmers, the propulsion force and the swimmer-swimmer interactions. Both concentration regimes are discussed to pinpoint the importance of interactions between swimmers for reduction of viscosity.

To reflect the settings of the physical experiments in [3] and [1] further, we studied the suspension at moderate concentrations of approximately 10% by volume. At such concentrations, the numerical analysis is the only available tool. The major difficulty in the theoretical analysis is the dependence of the apparent instantaneous viscosity on the distribution of the swimmers in the fluid domain. The distribution changes with time due to interaction of the swimmers with the ambient flow and other swimmers. In direct numerical simulations, to obtain accurate values for the effective viscosity, we average the instantaneous apparent viscosity over extended periods of time.

First, to validate the model and to analyze accuracy of the numerical method we performed a number of tests for the dynamics of a swimmer in the proximity of a wall or another swimmer. We observed the attraction of a swimmer to another swimmer and a swimmer to the wall. The attraction in both cases is only short term. A swimmer next to a wall, while getting closer to the wall, will slowly rotate and swim away from the wall. Two nearby swimmers will swim away from one another once their positions become offset from the mirror image configuration (see Fig. 6). These numerical results agree with the physical observations for *Escherichia coli* [31], *Bacillus subtilis* [4], and *Volvox* [20]. At the same time, the results shed light on the details of the swimmer-swimmer and swimmer-wall interactions.

Second, we performed a number of numerical simulations at the moderate concentrations where we computed the effective shear viscosity of a suspension of swimmers in a layer between two solid walls undergoing a shearing motion with relative velocity $2v$. We analyzed the dependence of the effective viscosity on the velocity v and the propulsion strength of the swimmers, f_p . Using an analytical scaling argument we demonstrated that the effective viscosity depends only on the *propulsion-shear ratio* $\frac{f_p}{\mu v}$ (μ is viscosity of the ambient fluid) for a fixed shape of the domain and the swimmers. The simulations indicate that the effective shear viscosity decays linearly as a function of the propulsion-shear ratio (for small values of $\frac{f_p}{\mu v}$). The same linear trend continues for negative values of the propulsion strength, which corresponds to microswimmers swimming in the opposite direction, i.e. pullers instead of pushers. For larger values of the propulsion-shear ratio a deviation from the linear trend was observed and explained by the finite size of the container.

The paper outline is as follows. In Section 2 we present a mathematical model for a swimmer in a fluid. We write down the complete set of PDEs and motivate each of the modeling assumptions. In section 2.3 we prove dependence of the effective shear viscosity on the propulsion-shear ratio. In Section 3.1 we define the instantaneous ap-

parent viscosity and the effective shear viscosity, which coincide for homogeneous fluids but are generally different for inhomogeneous ones. In Section 4 we briefly describe the numerical method, technical difficulties and their solutions followed by the computational results for dynamics of interacting swimmers and the effective shear viscosity for a suspension of swimmers. Section 4.5 relates the time and size units in our numerical simulations to the units in physical experiments [4]. Finally, in Section 5 we summarize the results of our analysis. In appendix A we present the variational formulation for the model and demonstrate its well-posedness.

2 Mathematical model of a swimmer

We present the PDE model for a microswimmer in a Stokesian fluid in Section 2.1 and motivate model assumptions in Section 2.2. The model is written in two dimensions but it can be readily extended to three dimensions. Although this PDE model was developed independently, reference should be made to the earlier works of Shelley and Saintillan [22] as well as Short, et al. [32]. Notable differences with [22] and [32] are that tractions are prescribed only on part of the boundary and collisions rules are different (no collisions in [32]).

2.1 The PDE model for the swimmer

Let $\Omega \subset \mathbb{R}^2$ be a bounded domain with a smooth boundary representing the container of the fluid with swimmers. Each swimmer is modeled as an ellipse S^i , $i = 1, \dots, N$, with the center at \mathbf{x}_c^i , and the orientation \mathbf{d}^i of the longest semiaxis, see Fig. 1. Here and below the superscript i indicates the index of the swimmer.

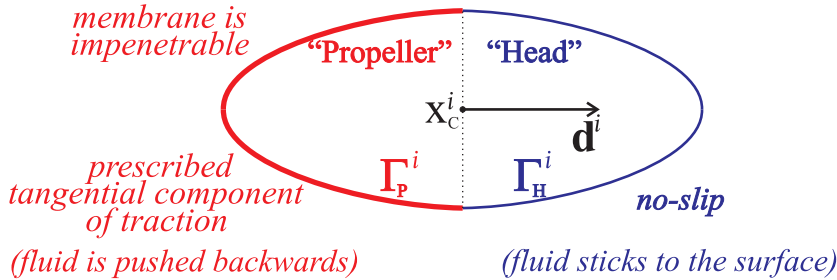


Fig. 1 Illustration of an i -th swimmer with two parts of the boundary: Γ_H^i and Γ_P^i . On the front part Γ_H^i of the swimmer (H stands for “head”) the fluid sticks to the surface. On the back part of the swimmer Γ_P^i (P stands for “propeller”) the fluid cannot penetrate the boundary of the swimmer. Also, the fluid is pushed backwards on Γ_P^i due to a prescribed tangential component of traction.

The motion of the fluid surrounding the swimmers is governed by the incompressible stationary Stokes equation

$$\begin{cases} \mu \Delta \mathbf{u} = \nabla p \\ \operatorname{div}(\mathbf{u}) = 0 \end{cases} \quad \text{in } \Omega_F := \Omega \setminus \bigcup_i S^i, \quad (1)$$

where \mathbf{u} is the fluid velocity, p is the pressure, and μ is viscosity. The boundary of the fluid domain Ω_F includes boundaries of the swimmers, Γ_H^i and Γ_P^i , and the boundary of the container, $\partial\Omega$. The following boundary conditions are imposed:

$$\mathbf{u}(\mathbf{x}) = \mathbf{g}(\mathbf{x}) \quad \text{for } \mathbf{x} \in \partial\Omega, \quad (2)$$

$$\mathbf{u}(\mathbf{x}) = \mathbf{u}_C^i + \omega^i \times (\mathbf{x} - \mathbf{x}_C^i) \quad \text{for } \mathbf{x} \in \Gamma_H^i, \quad (3)$$

$$\begin{cases} (\mathbf{u}(\mathbf{x}) - [\mathbf{u}_C^i + \omega^i \times (\mathbf{x} - \mathbf{x}_C^i)]) \cdot \mathbf{n} = 0 \\ \boldsymbol{\tau} \sigma(\mathbf{u}, p) \mathbf{n} = -f((\mathbf{x} - \mathbf{x}_C^i) \cdot \mathbf{d}^i) (\boldsymbol{\tau} \cdot \mathbf{d}^i) \end{cases} \quad \text{for } \mathbf{x} \in \Gamma_P^i, \quad (4)$$

$$\mathbf{F}_H^i + \mathbf{F}_P^i = 0 \quad (\text{balance of forces}), \quad (5)$$

$$\mathbf{T}_H^i + \mathbf{T}_P^i = 0 \quad (\text{balance of torques}). \quad (6)$$

Here, the instantaneous translational, \mathbf{u}_C^i and rotational, ω^i , velocities are additional unknowns. The symbols \mathbf{n} and $\boldsymbol{\tau}$ denote the unit normal and unit tangent to the surface. The stress tensor $\sigma(\mathbf{u}, p)$ is defined by

$$\sigma(\mathbf{u}, p) := 2\mu D(\mathbf{u}) - p\mathbf{I}, \quad D(\mathbf{u}) := \frac{1}{2} (\nabla \mathbf{u} + (\nabla \mathbf{u})^T), \quad (7)$$

where \mathbf{I} is the identity matrix.

The known scalar function f in (4) defines the propulsion model (see e.g., (12)). The known vector function \mathbf{g} in (2) is the velocity of the container boundary. The viscous forces \mathbf{F}_H^i , \mathbf{F}_P^i and torques \mathbf{T}_H^i , \mathbf{T}_P^i on Γ_H^i and Γ_P^i , respectively, are given by

$$\mathbf{F}_H^i := \int_{\Gamma_H^i} \sigma(\mathbf{u}, p) \mathbf{n} \, d\mathbf{x}, \quad \mathbf{F}_P^i := \int_{\Gamma_P^i} \sigma(\mathbf{u}, p) \mathbf{n} \, d\mathbf{x} \quad (8)$$

and

$$\mathbf{T}_H^i := \int_{\Gamma_H^i} (\mathbf{x} - \mathbf{x}_C^i) \times \sigma(\mathbf{u}, p) \mathbf{n} \, d\mathbf{x}, \quad \mathbf{T}_P^i := \int_{\Gamma_P^i} (\mathbf{x} - \mathbf{x}_C^i) \times \sigma(\mathbf{u}, p) \mathbf{n} \, d\mathbf{x}. \quad (9)$$

The PDE problem (1)-(6) defines the so-called *instantaneous problem*. The existence and uniqueness of the solution is outlined in Appendix A.

The dynamics of the swimmers, defining the evolution of the fluid domain $\Omega_F(t)$, is given by the following ODEs:

$$\begin{cases} \frac{d}{dt} \mathbf{x}_C^i(t) = \mathbf{u}_C^i(t), \\ \frac{d}{dt} \mathbf{d}^i(t) = \mathbf{d}^i(t) \times \omega^i(t) \end{cases} \quad (10)$$

with the initial conditions

$$\mathbf{x}_C^i(0) = \mathbf{x}_C^{i,0}, \quad \mathbf{d}_C^i(0) = \mathbf{d}_C^{i,0}, \quad \|\mathbf{d}_C^{i,0}\| = 1. \quad (11)$$

2.2 Discussion and motivation for the PDE model

Modeling of the fluid motion by the incompressible stationary Stokes equations (1) is a fairly standard reduction from the Navier-Stokes equations for small Reynolds number, $\mathcal{R}e := \frac{\rho V L}{\mu} \ll 1$. Here ρ is the density of the fluid ($\rho \approx 1 \text{g/cm}^3$), V and L are representative velocity and size in the problem. For instance, on the scale of self-propelled bacteria, such as *Bacillus subtilis* ($5 \mu\text{m}$ in length and $.7 \mu\text{m}$ in width) swimming with the velocity up to $100 \mu\text{m/sec}$, we obtain $\mathcal{R}e \approx 10^{-4} \ll 1$.

The boundary condition (2) indicates that the fluid sticks to the walls of the container Ω , which are moving with velocity \mathbf{g} . This is the standard boundary condition for solid walls. It can also be applied to the case of microswimmers in a thin film. The boundary $\partial\Omega$, here, would be the fluid-air interface. The reason for using the no-slip boundary condition would be the experimental evidence that microorganisms produce a surfactant that solidifies the interface [23] and effectively creates no-slip conditions. The solid-like behavior of the interface was also evidenced in [33], where dry friction like behavior was observed for a micro gear touching interface, which manifests solid surface.

The boundary condition (3) is similar to the condition (2) in that the fluid sticks to the surface Γ_H^i . But unlike $\partial\Omega$, the boundary Γ_H^i is moving with translational velocity \mathbf{u}_C^i and rotational velocity ω^i that are not known a priori and need to be found in the process of solving (1)-(6).

The first boundary condition in (4) indicates that the fluid cannot flow through the surface of the swimmer. The second condition describes a force that acts on the fluid and pushes it backward, as a result propelling the swimmer forward. Thus, we have just enough boundary conditions on Γ_P^i for solvability of the problem. Note that the form of the right-hand side in (4) indicates that the propulsion of the swimmer is coordinate invariant. An example of the scalar function f is the ‘‘uniform’’ distribution of force along the boundary:

$$\tau \sigma(\mathbf{u}, p) \mathbf{n} = -f((\mathbf{x} - \mathbf{x}_C^i) \cdot \mathbf{d}^i) (\boldsymbol{\tau} \cdot \mathbf{d}^i) := \frac{-f_p}{|\Gamma_P^i|} (\boldsymbol{\tau} \cdot \mathbf{d}^i), \quad (12)$$

where f_p is the *total force of the propulsion*:

$$f_p = \int_{\Gamma_P^i} f((\mathbf{x} - \mathbf{x}_C^i) \cdot \mathbf{d}^i) dx. \quad (13)$$

Boundary conditions (5) and (6) indicate that all swimmers are self-propelled as opposed to moving due to an external force (e.g., gravity). One can obtain these equations from Newton’s second law, noting that in the Stokes regime the inertial forces are negligible compared to the viscous forces (see [34] for more details).

From a modeling point of view an important feature of microswimmers propelled by flagella is the clockwise rotation of the swimmer’s body around its axis due to hydrodynamic torque resulting from the counter-clockwise rotation of the flagella. In two-dimensional model there cannot be rotation around the axis. Also, the rotation of bacteria in thin films can be freely neglected due to proximity of the fluid-air interface above and below versus only on side of bacteria, as considered in [31]. On the other hand, should an analogous three-dimensional model be constructed this feature should be added in the definition of the tangential component of tractions on the part of the boundary responsible for the self-propulsion.

2.3 Scaling observation

The following observation will simplify the future analysis. Consider two initial value problems (1)-(11) in the same domain Ω and with the same initial data (i.e., positions of the swimmers $\{\mathbf{x}_C^i(0), \mathbf{d}^i(0)\}_{i=1}^N$) but with different boundary conditions:

Problem I: The boundary data are

$$\mathbf{g}^I(t, \mathbf{x}) \quad \text{and} \quad f^I(s). \quad (14)$$

Problem II: The boundary data are

$$\mathbf{g}^{II}(t, \mathbf{x}) = \lambda \mathbf{g}^I(t/\lambda, \mathbf{x}) \quad \text{and} \quad f^{II}(s) = \lambda f^I(s). \quad (15)$$

We use superscripts I and II to denote solutions to the above problems. The following result is verified by the directed substitution.

Lemma 1 (Scaling) *Let functions $\mathbf{u}^I(t, \mathbf{x})$, $p^I(t, \mathbf{x})$ and positions of the swimmers $\{\mathbf{x}_C^{i,I}(t), \mathbf{d}^{i,I}(t)\}_{i=1}^N$ be solution to the first problem. Then, the functions*

$$\mathbf{u}^{II}(t, \mathbf{x}) := \lambda \mathbf{u}^I(t/\lambda, \mathbf{x}), \quad p^{II}(t, \mathbf{x}) := \lambda p^I(t/\lambda, \mathbf{x}) \quad (16)$$

and the positions of the swimmers,

$$\mathbf{x}_C^{i,II}(t) = \mathbf{x}_C^{i,I}(t/\lambda), \quad \mathbf{d}^{i,II}(t) = \mathbf{d}^{i,I}(t/\lambda), \quad (17)$$

are solutions to the second problem.

Remark 1 *The statement of Lemma 1 can be phrased as follows. Simultaneously increasing the propulsion force $f(\cdot)$ of the swimmers and the fluid velocity $\mathbf{g}(\mathbf{x})$ by a factor of λ leads to swimmers moving along the same trajectories but λ times faster. The corresponding viscous forces are increased by a factor λ .*

Remark 2 *A rotational diffusion may be used to model the Brownian motion or tumbling. This diffusion introduces a new time-scale which breaks up the scaling result of Lemma 1.*

3 Effective viscosity

In the theory of fluid dynamics one of the primary objects of interest is the relation between the applied forces (stress) and the observed fluid flow (strain rate). For Newtonian fluids this relationship is linear:

$$\boldsymbol{\sigma}(\mathbf{x}) = 2\mu D(\mathbf{u}(\mathbf{x})) - p(\mathbf{x})\mathbf{I} \quad \text{for } \mathbf{x} \in \Omega_F. \quad (18)$$

For non-Newtonian fluids (18) does not hold with the same value of μ . Hence, assuming that one still desires to characterize the relation between the stress and the strain rate in the form similar to (18), the viscosity μ should be permitted to vary.

In the most general case, μ will depend on the form of the flow, i.e. $\mu(D(\mathbf{u}))$. This is not very informative, as in this case the relation (18) is equivalent to $\boldsymbol{\sigma} = F(D(\mathbf{u}))$, where $F(\cdot)$ is some function. Thus, to characterize the relation between the stress and the strain rate, one should specify the function $F(\cdot)$.

To avoid this problem, we accept the fact that the general relation between the bulk stress and the bulk strain rate greatly depends on the type of the fluid flow. Thus, we will limit ourselves to a rather specific, but experimentally intuitive definition along the lines, proposed by Batchelor [35]:

“We shall consider here only the important and representative case in which the suspension is confined between two parallel rigid planes in steady relative shearing motion, with the stress being observed as the force per unit area on a section of one boundary with linear dimensions large compared with particle spacing.”

3.1 Definition of effective viscosity and instantaneous apparent viscosity

Consider a fluid (or a complex fluid, such as a suspension of active or passive particles in the fluid) between two solid plates a distance $2H$ apart, see Fig. 2. We induce a shearing motion on the boundary by moving the top plate to the right with velocity $v\mathbf{e}_1$ and the bottom plate to the left with velocity $-v\mathbf{e}_1$. We prescribe the periodic conditions on the vertical left and right boundaries. The effective shear viscosity, being a measure of friction in the fluid, should be defined in terms of the total viscous forces

$$\mathbf{F}_T := \int_{\Gamma_T} \sigma(\mathbf{u}, p) \mathbf{n} \, d\mathbf{x} \quad \text{and} \quad \mathbf{F}_B := \int_{\Gamma_B} \sigma(\mathbf{u}, p) \mathbf{n} \, d\mathbf{x}, \quad (19)$$

acting on the top (Γ_T) and the bottom (Γ_B) plates, respectively, and should scale correctly with the dimensions of the domain. These considerations suggest the following quantity, dubbed as the *instantaneous apparent viscosity*:

$$\bar{\mu}(v; t) := \frac{H}{Lv} (\mathbf{F}_T(t) - \mathbf{F}_B(t)) \cdot \mathbf{e}_1, \quad (20)$$

where L is the length of the plate on which viscous forces \mathbf{F}_T and \mathbf{F}_B are acting and $\frac{v}{2H} = \dot{\epsilon}$ is the shear rate of the background flow created by the motion of the top and bottom plates.

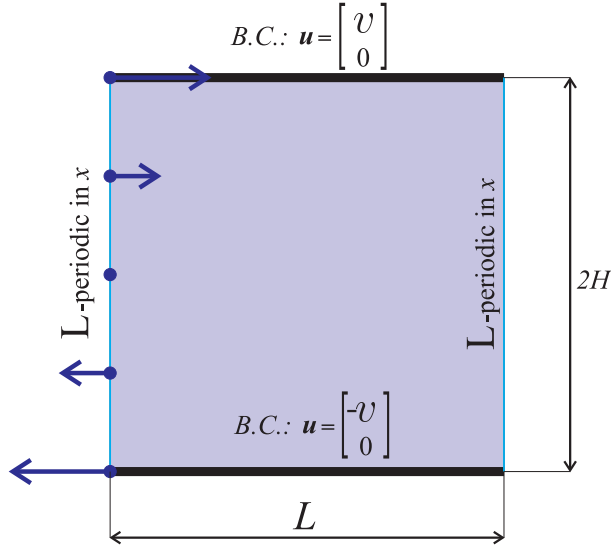


Fig. 2 Schematic illustration of shear flow between two plates.

For homogeneous fluids the quantity (20) does not depend on time since the viscous forces \mathbf{F}_T and \mathbf{F}_B do not change with time. For inhomogeneous fluid there are additional challenges. For instance, for a suspension of passive or active inclusions, the value of $\bar{\mu}(v; t)$ will be different depending on the concentration and distribution of inclusions. For a suspension of active inclusions, such as swimmers, it will also depend on the propulsion strength of the swimmers. Moreover, changing the propulsion strength from f_p to $-f_p$ will change the value of $\bar{\mu}(v; t)$ in a nontrivial way. In general, this value will not remain the same and will not simply change sign. For this reason, we call the quantity in (20) the instantaneous apparent viscosity and not the effective viscosity, which will be defined later. The word *instantaneous* indicates that $\bar{\mu}(v; t)$ is computed at a particular instance of time and depends on a particular configuration of swimmers. The word *apparent* indicates the nontrivial dependence on the propulsion strength f_p . This dependence will be analyzed later in section 3.2.1.

We would like to define the effective viscosity as a material property independent of the configuration of swimmers. Thus, we define the *effective viscosity* as a time average of the instantaneous apparent viscosity

$$\hat{\mu}(v) := \lim_{T \rightarrow \infty} \frac{1}{T} \int_0^T \bar{\mu}(v; t) dt. \quad (21)$$

We assume that this time-averaged quantity does not depend on the initial configuration of swimmers. Verification this assumption is a separate research topic, which we leave for possible future analysis.

3.2 Estimates and observations for the instantaneous apparent viscosity

Here we make some analytic observations regarding the instantaneous apparent viscosity. First, we make use of the scaling observation, Remark 1. This observation tells us that the instantaneous apparent viscosity, as defined by (20), takes the same value for problems *I* and *II*, (14)-(15), at times t/λ and t , respectively:

$$\begin{aligned} \bar{\mu}^{II}(\lambda v, \lambda f_p; t/\lambda) &= \frac{H}{L\lambda v} \left(\mathbf{F}_T^{II}(t/\lambda) - \mathbf{F}_B^{II}(t/\lambda) \right) \cdot \mathbf{e}_1 = \\ &= \frac{H}{Lv} \left(\mathbf{F}_T^I(t) - \mathbf{F}_B^I(t) \right) \cdot \mathbf{e}_1 = \bar{\mu}^I(v, f_p; t). \end{aligned} \quad (22)$$

Hence, the effective viscosities, being time averages of the instantaneous apparent viscosities, also, match for the problems *I* and *II*:

$$\begin{aligned} \hat{\mu}^{II}(\lambda v, \lambda f_p) &= \lim_{T \rightarrow \infty} \frac{1}{T} \int_0^T \bar{\mu}^{II}(\lambda v, \lambda f_p; t/\lambda) dt = \\ &= \lim_{T \rightarrow \infty} \frac{1}{T} \int_0^T \bar{\mu}^I(v, f_p; t) dt = \hat{\mu}^I(v, f_p). \end{aligned} \quad (23)$$

This means that the effective viscosity of a suspension of swimmers depends only on the ratio of the propulsion strength f_p to the shear rate defined by v , i.e.

$$\hat{\mu} \left(\frac{v}{f_p} \right) := \hat{\mu} \left(\frac{v}{f_p}, 1 \right) = \hat{\mu} \left(1, \frac{f_p}{v} \right). \quad (24)$$

The nondimensional analog of $\frac{f_p}{v}$ is $\frac{f_p}{\mu v}$. Due to its importance we shall refer to the ratio $\frac{f_p}{\mu v}$ as the *propulsion-shear ratio*.

3.2.1 The apparent viscosity for the instantaneous problem

In this section we identify the dependence of the instantaneous apparent viscosity on the propulsion strength f_p of the swimmers for a given distribution of swimmers. We will consider three instantaneous problems **A**, **B** and **C** given by (1)-(6) in the same fluid domain Ω_F but with different boundary conditions:

- A. Active swimmers + Shear:** $v^A = v$ and $f_p^A = f_p$.
- B. Passive/dormant swimmers + Shear:** $v^B = v$ and $f_p^B = 0$.
- C. Active swimmers + No shear:** $v^C = 0$ and $f_p^C = f_p$.

Due to linearity of the Stokes equations (1) the solution (\mathbf{u}^A, p^A) to the problem **A** is a sum of the solutions (\mathbf{u}^B, p^B) and (\mathbf{u}^C, p^C) to the problems **B** and **C**:

$$\mathbf{u}^A(\mathbf{x}) = \mathbf{u}^B(\mathbf{x}) + \mathbf{u}^C(\mathbf{x}) \quad \text{and} \quad p^A(\mathbf{x}) = p^B(\mathbf{x}) + p^C(\mathbf{x}). \quad (25)$$

We have a similar relation for the forces on the top and bottom plates. Thus, the expression that enters the definition (20) of the instantaneous apparent viscosity is

$$\mathbf{F}_T^A(v, f_p) - \mathbf{F}_B^A(v, f_p) = \left(\mathbf{F}_T^B(v) - \mathbf{F}_B^B(v) \right) + \left(\mathbf{F}_T^C(f_p) - \mathbf{F}_B^C(f_p) \right). \quad (26)$$

Here we explicitly indicated that the forces depend on the shear velocity v and the propulsion strength of the swimmers. Inserting this in definition (20), we obtain

$$\begin{aligned} \bar{\mu}^A(v, f_p) &= \frac{H}{Lv} \left(\mathbf{F}_T^A(v, f_p) - \mathbf{F}_B^A(v, f_p) \right) \cdot \mathbf{e}_1 = \\ &= \frac{H}{Lv} \left(\mathbf{F}_T^B(v) - \mathbf{F}_B^B(v) \right) \cdot \mathbf{e}_1 + \frac{H}{Lv} \left(\mathbf{F}_T^C(f_p) - \mathbf{F}_B^C(f_p) \right) \cdot \mathbf{e}_1 = \\ &= \bar{\mu}^B(v) + \frac{1}{v} \bar{\eta}(f_p), \end{aligned} \quad (27)$$

where

$$\frac{1}{v} \bar{\eta}(f_p) := \bar{\mu}^A(v, f_p) - \bar{\mu}^B(v) = \frac{H}{Lv} \left(\mathbf{F}_T^C(f_p) - \mathbf{F}_B^C(f_p) \right) \cdot \mathbf{e}_1 \quad (28)$$

is the contribution to the instantaneous apparent viscosity due to self-propulsion.

3.3 Effective shear viscosity for a suspension of swimmers in the dilute regime

Consider a suspension of swimmers in the dilute regime: the fluid domain is sufficiently large and swimmers are sufficiently far apart from one another. Thus, the dilute assumptions are as follows: (i) individual swimmers interact only with the background flow and do not interact with one another, (ii) only orientations of swimmers play role in the effective viscosity. We use decomposition (27) of the instantaneous apparent viscosity to derive the following results.

Let $\omega(\theta)$ be the rotational velocity of a swimmer as a function of angle θ between the swimmer major semiaxis and the x -axis. Assume that shear motion is along the x -axis.

Lemma 2 *The rotational velocity of swimmers is an even function of θ , i.e.*

$$\omega(\theta) = \omega(-\theta). \quad (29)$$

Proof Indeed, the rotation of swimmers is entirely due to the background flow and does not depend on the propulsion strength f_p of the swimmers. That is the rotational velocity $\omega = \omega(\theta, \dot{\epsilon})$ is only a function of the orientation of the swimmer and the shear rate $\dot{\epsilon}$ of the background flow.

Due to reversibility of the Stokes flow, we get

$$\omega(\theta, -\dot{\epsilon}) = -\omega(\theta, \dot{\epsilon}). \quad (30)$$

Consider the reflection of the problem across x -axis. Such reflection maps

1. orientation θ to $-\theta$,
2. the flow with shear rate $\dot{\epsilon}$ to the flow with shear rate $-\dot{\epsilon}$,
3. angular velocity ω to $-\omega$ (due to change of the clockwise orientation)

Using the mapping 1-3 above and (30) we get the desired result (29)

$$\omega(-\theta, \dot{\epsilon}) = -\omega(\theta, -\dot{\epsilon}) = -(-\omega(\theta, \dot{\epsilon})) = \omega(\theta, \dot{\epsilon}).$$

Let $p(\theta)$ be the density function for the portion of time that a swimmer spends at the angle θ ,

$$\int_{-\pi}^{\pi} p(\theta) d\theta = 1.$$

Here the average can be taken over the time it takes a swimmer to complete a full rotation in the shear flow. Note that $p(\theta)$ is the same for all swimmers regardless of their initial orientation.

Lemma 3 *The density function $p(\theta)$ is an even function of θ , i.e.*

$$p(\theta) = p(-\theta). \quad (31)$$

Proof The statement (31) follows from Lemma 2 and the conservation of angular flux condition

$$p(\theta)\omega(\theta) = \text{constant for all } \theta, \quad (32)$$

which says that the average flux of orientations of swimmers through the angle θ does not depend on θ .

Indeed, (32) holds due to every swimmer rotating periodically in the same direction (clockwise for $v > 0$, counter-clockwise for $v < 0$). Thus, the number of swimmers passing through orientations θ_1 and θ_2 on average over time is the same.

From (32) and (29) we have

$$p(\theta)\omega(\theta) = p(-\theta)\omega(-\theta) = p(-\theta)\omega(\theta).$$

Dividing through by $\omega(\theta)$ we get (32).

Now we consider the contribution of self-propulsion to the instantaneous apparent viscosity $\bar{\mu}(f_p; t)$ as introduced in (27) and (28).

Lemma 4 *The total contribution, $\frac{1}{v}\hat{\eta}(f_p) := \hat{\mu}(v, f_p) - \hat{\mu}(v, 0)$, of self-propulsion to the effective viscosity is zero:*

$$\begin{aligned} \frac{1}{v}\hat{\eta}(f_p) &= \frac{1}{v} \lim_{T \rightarrow \infty} \frac{1}{T} \int_0^T \bar{\eta}(f_p; t) dt = \\ &= \frac{H}{Lv} \lim_{T \rightarrow \infty} \frac{1}{T} \int_0^\infty \left(\mathbf{F}_T^C(f_p; t) - \mathbf{F}_B^C(f_p; t) \right) \cdot \mathbf{e}_1 dt = 0. \end{aligned} \quad (33)$$

Proof The contribution of N swimmers to $\bar{\eta}(f_p; t)$ is a sum of contributions $\bar{\eta}_1(f_p, \theta_i(t))$ of individual swimmers:

$$\bar{\eta}(f_p; t) = \sum_{i=1}^N \bar{\eta}_1(f_p, \theta_i(t)).$$

From the symmetry of the flow, the contribution $\bar{\eta}_1(f_p, \theta)$ is an odd function of θ :

$$\bar{\eta}_1(f_p, \theta) = -\bar{\eta}_1(f_p, -\theta).$$

Hence, the contribution of all swimmers to the instantaneous apparent viscosity due to self-propulsion is

$$\begin{aligned} \hat{\eta}(f_p) &= \lim_{T \rightarrow \infty} \frac{1}{T} \int_0^T \sum_{i=1}^N \bar{\eta}_1(f_p, \theta_i(t)) dt = N \int_{-\pi}^{\pi} p(\theta) \bar{\eta}_1(f_p, \theta) d\theta = \\ &= N \int_{-\pi}^0 p(\theta) \bar{\eta}_1(f_p, \theta) d\theta + N \int_0^{\pi} p(\theta) \bar{\eta}_1(f_p, \theta) d\theta = \\ &= -N \int_0^{\pi} p(\theta) \bar{\eta}_1(f_p, \theta) d\theta + N \int_0^{\pi} p(\theta) \bar{\eta}_1(f_p, \theta) d\theta = 0. \end{aligned} \quad (34)$$

This proves the assertion of the lemma.

Note that $\hat{\eta}(f_p) = 0$ independently of the initial orientations of the swimmers. This is due to the first line of (34), which says that the time average of the contribution of each swimmer $\bar{\eta}_1(f_p, \theta_i(t))$ is equal to the average over one full rotation of the swimmer. The later one does not depend on the initial orientation of the swimmer.

From the definition of the effective viscosity (21), decomposition of instantaneous apparent viscosity (27), independence of the dynamics of the orientations of swimmers of the propulsion strength and, finally, Lemma 4 we get the following statement.

Theorem 1 *The effective viscosity $\hat{\mu}(v, f_p)$, defined by (21), of a suspension of swimmers with propulsion strength f_p , defined by (13), interacting only with the background shear flow (i.e., no swimmer-swimmer interactions) is independent on the propulsion strength f_p .*

Remark 3 *The immediate consequence of Theorem 1 is that in the dilute limit the effective viscosities of suspensions of active and passive swimmers are the same.*

Remark 4 *The result of Theorem 1 is based on a different set of assumptions than Ishikawa and Pedley [21], where swimmers have a shifted center of gravity. Our swimmers centers of gravity is the same as their geometric center. In fact, our result explains why Ishikawa and Pedley could not obtain decrease of viscosity for swimmers with “neutral” center of gravity.*

Remark 5 *Adding to the model the rotational diffusion (either due to Brownian motion or tumbling), in the absence of the swimmer-swimmer interactions, would breaks up the symmetry (31) and lead to a preferential alignment of swimmers. Depending on the sign of the propulsion strength f_p , the flow due to swimmers helps ($f_p > 0$) or resists ($f_p < 0$) the background shearing motion. This explains the results of [30], where the decrease of effective viscosity is observed in the presence of rotational diffusion.*

4 Numerical modeling and analysis

We solve the ODEs (10) using the forward Euler method with variable time step Δt_n (see more on the choice of the time-step in Section 4.2). On each time step t_n , using positions $\mathbf{x}_C^i(t_n)$ and orientations $\mathbf{d}^i(t_n)$ of swimmers, we find their new translational and rotational velocities by solving the problem (1)-(6). After that, we update positions of the swimmers, assuming constant velocities on the time interval $(t_n, t_n + \Delta t_n)$:

$$\mathbf{x}_C^i(t_{n+1}) = \mathbf{x}_C^i(t_n) + \Delta t_n \mathbf{v}_C^i(t_n). \quad (35)$$

Since our spatial discretization method is first-order accurate for stresses in terms of the mesh size, the first-order accurate time integration method is sufficient to balance spatial and temporal errors.

4.1 Solution of the instantaneous problem

Efficient and accurate solution of the PDE problem (1)-(6) on each time step is required for computing the viscosity of the suspension. We use the recently developed Mimetic Finite Difference (MFD) method [36]. Since the MFD method for the Stokes problem is a new method, we give a short comparative description of this method and some other popular methods.

4.1.1 Short description of MFD method

The MFD method combines mesh flexibility of the Finite Volume (FV) methods with analytical power of Finite Element (FE) methods. To some extent it can be viewed as an extension of FE methods to unstructured polygonal (polyhedral in three dimensions) meshes. The mesh flexibility simplifies mesh generation around swimmers that may have complicated shapes. The major difference between the MFD and FE methods lies in definition of basis functions. The FE methods define them explicitly everywhere in the computational domain. The MFD method specifies the basis functions only on mesh edges. This reduction of topological complexity has a number of important consequences for numerical modeling of complex phenomena.

First, the MFD method minimizes the number of discrete unknowns (compared to the FE method) (a) by partitioning of the computation domain into smaller number of elements that are polygons and (b) by using velocity and pressure degrees of freedom only where they are needed for accuracy and stability of the discretization. For example, the MFD method on a square mesh with N mesh vertices uses about $2.5N$ velocity and N pressure unknowns. The FE methods on the same mesh and with roughly the same accuracy uses about $4N$ velocity and N pressure unknowns.

Second, the MFD method is built the same way on general polygonal meshes as on triangular meshes. Thus, it can be used on locally refined meshes with hanging nodes and on moving meshes with non-convex elements that are frequently used in numerical modeling. It was shown in [37] that the MFD method can be employed even when the mesh elements have curved faces. In this work, we use polygonal meshes near boundary of the swimmers (see Section 4.1.2) and make the computational mesh coarser far away from the swimmers. This approach increases accuracy in the areas of interest. The MFD method is the second-order accurate (with respect to the local mesh size) for the velocity and the first-order accurate for the pressure.

4.1.2 Mesh construction

In the simulations, we used a three-step algorithm for construction of the computational mesh. First, we construct a uniform square background mesh, i.e. the square domain of size 1 by 1 is divided into N^2 squares with sides $h = 1/N$.

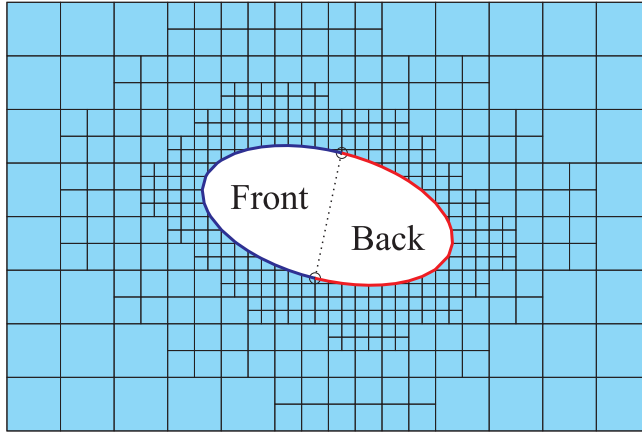


Fig. 3 A sample mesh near a swimmer. The computational domain is around the swimmer and is colored light blue. The mesh is coarsened away from the swimmer. Notice that the mesh elements adjacent to the swimmer are polygons with 3, 4 and 5 vertices.

Second, we overlap the background mesh with the ellipses representing swimmers. For this, we find the points of intersection of the ellipses with the edges of the background mesh. These points are connected by straight edges and added to the new mesh. The mesh elements inside the ellipses are then thrown out. As a result, the boundary of the ellipses is approximated with the second-order accuracy and the resulting mesh is polygonal (see Fig. 3).

Third, we coarsen the mesh by grouping the mesh elements whose centers are at least $2h$ away from the swimmers into square mesh elements with sides $2h$. This process can be repeated by grouping the mesh elements whose centers are at least $4h$ away from the swimmers into square mesh elements with sides $4h$. This strategy leaves the mesh intact in the neighborhood of swimmers where spacial variation of flow is the largest.

4.2 Choosing the time step

There are several factors that determine the size of the time step Δt_n . For moderate concentrations of swimmers ($\sim 10\%$ by volume) the crucial point to be addressed is collision of swimmers. For this, the relative displacements of swimmers on each time step should be small compared to their pairwise distances. Due to the hydrodynamic attraction of swimmers it is common to see pairs of swimmers arbitrarily close to one another. This requires to use extremely small time steps; therefore, such an approach is not practical.

We implemented a balanced algorithm for choosing the time step. First, we fix the upper Δt_{upper} and the lower Δt_{lower} bounds for the time step. Then, we pick the size

of the time step Δt such that

$$\Delta t_{\text{upper}} \geq \Delta t \geq \Delta t_{\text{lower}}$$

and the swimmers cannot get closer than the mesh size h to one another. If both criteria cannot be satisfied, we set $\Delta t := \Delta t_{\text{lower}}$ and apply the collision algorithm described in the next subsection.

Numerical experiments have shown that $\Delta t_{\text{upper}} := .01$ and $\Delta t_{\text{lower}} := .001$ for the propulsion strength of swimmers $f_p = 1$ and the shear rate $\dot{\epsilon} = 1$ lead to smooth dynamics of the apparent viscosity (see Fig. 7). When $f_p > 1$, the time step is selected based on the scaling observation (see Remark 1). This remark implies that trajectories of swimmers for the case with $\dot{\epsilon} = 1$, $f_p = f_p^0$, $\Delta t = \Delta t^0$ will be close to that in the case with $\dot{\epsilon} = 1/\lambda$, $f_p = f_p^0/\lambda$, $\Delta t = \Delta t^0/\lambda$. We choose the scaling constant $\lambda = f_p$, i.e. we fix the propulsion strength of the swimmers. This leads to smaller values of the shear rate than in the base case. Therefore, our choice of the upper and lower bounds for the time step is $\Delta t_{\text{upper}} := .01/f_p$ and $\Delta t_{\text{lower}} := .001/f_p$.

4.3 Implementing collisions of swimmers

Dynamic change of the time step only minimizes probability of collisions and does not eliminate them completely. There are two popular methods for dealing with collisions of rigid objects. A group of methods use a short range repulsive force to push swimmers away from one another. The method employed in our simulations is used commonly in modeling of granular media [38] and is better suited for the problems with many bodies close to one another, where long time simulations are necessary.

Lubrication theory can be used to make asymptotically correct predictions for small pairwise distances $\delta \ll 1$ between swimmers. But the smallest allowed pairwise distance is tied together with the size of the time step, $\Delta t \sim \delta$. Since for many swimmers at concentration 9% by volume almost always there are swimmers next to one another, allowing too small pairwise distances would make time stepping prohibitively slow. In our analysis, we require swimmers to be approximately one mesh size apart. Lubrication theory would be more appropriate for a very detailed, short-term analysis of two swimmers near contact, than for an analysis of many swimmers where long-term collection of statistics is essential.

To avoid additional technical difficulties, we consider a small exclusion region around each swimmer. The exclusion region for the ellipse with major semi-axis a and b is defined as the ellipse with major semi-axis $a + h$ and $b + h$, respectively. Therefore, if the exclusion regions of two swimmers do not overlap, then these swimmers are guaranteed not to have a common mesh element adjacent to both. The collision is implemented as a soft collision of exclusion regions, where the place of mass is taken by the viscous drag coefficients of the ellipses.

Consider two ellipses in contact. The force of their interaction is directed along the normal to their surfaces at the point of the contact. The force $\mathbf{F}_{1,2}$ of the first swimmer S_1 onto the second swimmer S_2 is equal in magnitude and opposite in direction to $\mathbf{F}_{2,1}$, the force of S_2 onto S_1

$$\mathbf{F}_{1,2} = -\mathbf{F}_{2,1}. \quad (36)$$

To estimate the effect of the interaction force $\mathbf{F}_{2,1}$ on the motion of the swimmer S_1 , we compute the net force and the net torque applied to the swimmer:

$$\mathbf{F}_{\text{net}}^1 = \mathbf{F}_{2,1} \quad \text{and} \quad T_{\text{net}}^1 = \mathbf{F}_{2,1} \times (\mathbf{x} - \mathbf{x}_C^1). \quad (37)$$

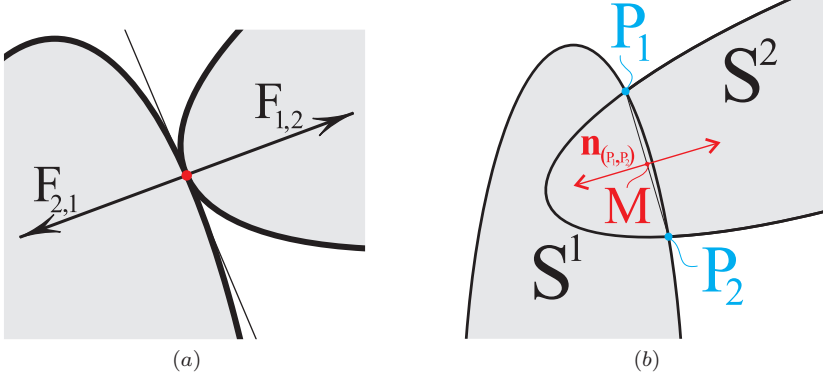


Fig. 4 Two ellipsoidal exclusion regions (containing swimmers) in contact (a) and two overlapping ellipsoidal exclusion regions (b).

The force $\mathbf{F}_{2,1}$ will be acting on swimmer S_1 as long as S_1 and S_2 are in contact. In the Stokes regime (where inertia is negligible compared to the viscous forces) the forces $\mathbf{F}_{2,1}$ and $\mathbf{F}_{1,2}$ will be only as strong as necessary to prevent mutual penetration of swimmers. Also, in the Stokes regime, the role of the mass is played by the viscous drag coefficients. We have three drag coefficients: two for translational motion along the major axes, γ_a and γ_b , and one for the rotational motion, γ_θ .

If \mathbf{d} is the direction of the major axis and \mathbf{d}_\perp is the direction of the minor axis, we may write the net force as $\mathbf{F}_{\text{net}}^1 = f_a \mathbf{d} + f_b \mathbf{d}_\perp$ and the motion of the ellipse as $\mathbf{u}_C^1 = u_a^1 \mathbf{d} + u_b^1 \mathbf{d}_\perp$ and ω^1 . The drag coefficients relate the forces acting on the ellipse with the motion of the ellipse as follows:

$$f_a = \gamma_a u_a^1, \quad f_b = \gamma_b u_b^1, \quad T_{\text{net}}^1 = \gamma_\theta \omega^1. \quad (38)$$

Now, suppose that at time t_0 we solved the Stokes problem for two swimmers S_1 and S_2 and found their velocities \mathbf{u}_C^i and ω^i , $i = 1, 2$. The positions of the swimmers at time $t_1 = t_0 + \Delta t$ are computed as follows:

$$\mathbf{x}_C^i(t_1) = \mathbf{x}_C^i(t_0) + \Delta \mathbf{x}^i, \quad \Delta \mathbf{x}^i = \Delta t \mathbf{u}_C^i(t_0).$$

Their orientations are incremented similarly by values $\Delta \theta^i$. By our assumptions, $\Delta t = \Delta t_{\text{lower}}$ and new positions result in overlap of ellipses (the protective regions).

In general, for two overlapping ellipses, there will be two points of intersection denoted by P_1 and P_2 (see Fig. 4(b)). The midpoint $M := (P_1 + P_2)/2$ will be considered as the point of the interaction. The interaction force (denoted by $\mathbf{n}_{(P_1, P_2)}$) will be assumed to act perpendicular to the line (P_1, P_2) as shown on the figure. Based on this, we can compute the corrected velocities of the swimmers:

$$\begin{aligned} u_a^1 &= \gamma_a^{-1} f_a = \gamma_a^{-1} \mathbf{d} \cdot \mathbf{n}_{(P_1, P_2)}, \\ u_b^1 &= \gamma_b^{-1} f_b = \gamma_b^{-1} \mathbf{d}_\perp \cdot \mathbf{n}_{(P_1, P_2)}, \\ \omega^1 &= \gamma_\theta^{-1} T_{\text{net}}^1 = \gamma_\theta^{-1} \mathbf{n}_{(P_1, P_2)} \times (M - \mathbf{x}_C^1). \end{aligned} \quad (39)$$

We are left to answer the question: How big should be the displacements $\Delta \mathbf{x}^1$ and $\Delta \theta^1$? Since we already computed the direction of the displacements the above question is reduced to the question of scaling: How big should be the scaling δ_t in $\Delta \mathbf{x}^1 = \delta_t \mathbf{u}_C^1$ and $\Delta \theta^1 = \delta_t \omega^1$?

We suggest to take δ_t so that the swimmers are slightly out of contact. For this, we select two points O^1 and O^2 on the boundaries of S^1 and S^2 , respectively, that are between P_1 and P_2 . For example, let us take O^1 to be the point, where the tangent line is parallel to the line passing through P_1 and P_2 . We choose the point O^2 in a similar fashion. Denoting the velocities of points O_1 and O_2 by \mathbf{u}_{O^1} and \mathbf{u}_{O^2} , respectively, we take

$$\delta_t := (1 + \alpha) \frac{(O^1 - O^2) \cdot \mathbf{n}_{(P_1, P_2)}}{(\mathbf{u}_{O^1} - \mathbf{u}_{O^2}) \cdot \mathbf{n}_{(P_1, P_2)}}.$$

Here $\alpha \geq 0$ is an analogue of a restitution coefficient (measure of bounce, i.e. elastic vs inelastic collision). It can, also, serve as a “reserve” to guaranty that after the procedure the ellipses do not overlap. In numerical simulations, we use $\alpha = 0.1$. which corresponds to soft collisions.

4.4 Dynamics: Interaction of swimmers

Here we present two numerical experiments for the hydrodynamic interaction of swimmers at the intermediate distances (distances of order of the size of the swimmer): a swimmer next to a wall (see Fig. 5a) and two side-by-side swimmers (see Fig. 5b). In both cases attraction due to a hydrodynamic interaction was observed.

This behavior can be explained, heuristically, by the fact that each swimmer acts as a force dipole (see (5)). It pushes fluid forward (ahead of itself) due to the no-slip condition on Γ_H and backward (behind itself) due to the thrust condition on Γ_P . Since the fluid is incompressible, it is being forced towards the swimmer on its sides creating lateral suction of sorts.

4.4.1 A swimmer next to a wall

In this numerical experiment, the swimmer was positioned distance 0.1 away parallel to a wall (see Fig. 5a). The lengths of the semi-axes of the swimmer were $a = 0.048$ and $b = 0.024$. The propulsion force is given by (12) with the propulsion strength $f_p = 1$.

The computed initial translational and rotational velocities of the swimmer were

$$\mathbf{u}_C^1 = \begin{bmatrix} 0.065 \\ -0.016 \end{bmatrix}, \quad \omega^1 = 0.061. \quad (40)$$

The vertical swimmer’s velocity is roughly quarter of its horizontal velocity indicating rather strong interaction with the wall. Over time the swimmer approaches the wall while simultaneously rotating away from it. When it has rotated sufficiently, it begins moving away from the wall.

We conclude that a swimmer positioned parallel to the wall is attracted to it and spends a significant amount of time swimming parallel to it. But it will not remain next to the wall indefinitely. The entire time spent near the wall, the swimmer rotates away and eventually swims away.

4.4.2 Two adjacent “mirror image” swimmers

In this experiment, we consider two swimmers with the length of the semi-axes $a = 0.048$ and $b = 0.024$, initially positioned parallel to the x -axes, with the centers on the same vertical line (see Fig. 5b):

$$\mathbf{x}_C^1 = \begin{bmatrix} 0.5 \\ 0.4 \end{bmatrix} \quad \text{and} \quad \mathbf{x}_C^2 = \begin{bmatrix} 0.5 \\ 0.6 \end{bmatrix}.$$

The swimmers are mirror images of one another with respect to the horizontal line $y = 0.5$.

The computed initial translational and rotational velocities of the swimmers were

$$\mathbf{u}_C^{1,2} = \begin{bmatrix} 0.066 \\ \pm 0.014 \end{bmatrix}, \quad \omega^{1,2} = \mp 0.02. \quad (41)$$

With time the swimmers approach one another, simultaneously rotating away from one another. This dynamics of two side-by-side swimmers is reminiscent of the dynamics of two well-separated “external pushers” in a similar configuration [34]. There is a difference between the well-separated and moderately separated regimes, however. In the well separated regime, the swimmers have enough time to rotate sufficiently away from one another for the translational correction (to swimming straight) due to the suction to be dominated by the vertical velocity for a free swimmer. In the moderate regime, the suction is too strong and the swimmers do not have enough time to rotate sufficiently outwards.

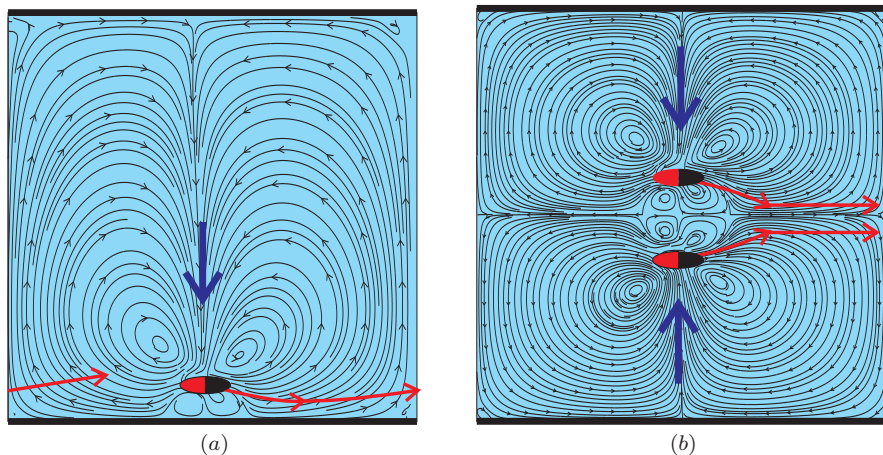


Fig. 5 Figure (a) shows the fluid flow for a single microswimmer next to a wall. Figure (b) shows the fluid flow for two swimmers side by side. The bold blue arrows indicate the direction of the fluid that pushes the swimmer closer to the wall (a) and the two swimmers closer to one another (b). The bold red lines with arrows indicate the trajectories that each of the swimmers will follow. Both (a) and (b) show the initial period of attraction (red line getting closer to the wall and two red lines getting closer to one another). The two swimmers in the mirror image configuration remain close to one another after this. The swimmer next to the wall rotates away from the wall to eventually get further and further away from it.

One can also compare the velocities (41) and (40). While the translational velocities in both cases are almost the same, the rotational velocity in (40) is roughly three times larger than in (41). This may explain the difference in the dynamics between swimmer next to a wall and two “mirror image” swimmers.

In Fig. 5(b) one can clearly see the trajectories of the swimmers converge and experience a sharp turn after which they become parallel. The swimmers will remain in this symmetrical configuration with distance 0.0664 between their centers and at the angles ∓ 0.28 (turned somewhat outwards) with the x -axes.

If the swimmers are initially not in a perfectly symmetric configuration, they eventually separate and swim away from one another. This type of dynamics is presented below.

4.4.3 Two adjacent “offset” swimmers

In this experiment, we consider two swimmers parallel to the x -axes with the centers offset from the same vertical line:

$$\mathbf{x}_C^1 = \begin{bmatrix} 0.55 \\ 0.40 \end{bmatrix} \quad \text{and} \quad \mathbf{x}_C^2 = \begin{bmatrix} 0.45 \\ 0.60 \end{bmatrix}.$$

This initial configuration of swimmers can be thought of as a perturbation of the “mirror image” configuration.

The computed initial translational and rotational velocities of the swimmers were

$$\mathbf{u}_C^1 = \begin{bmatrix} 0.0626 \\ 0.0047 \end{bmatrix}, \quad \omega^1 = -0.12, \quad \mathbf{u}_C^2 = \begin{bmatrix} 0.0740 \\ -0.0064 \end{bmatrix}, \quad \omega^2 = -0.11. \quad (42)$$

Initially, both of the swimmers rotate in the same direction, clockwise. The direction of the rotation is determined by the swimmer which is ahead of the other one, the bottom swimmer in this configuration. Thus, the second (top) swimmer rotates towards the first one (see the streamlines in Fig. 6). This swimmer two will cross the trajectory of the first swimmer, behind it, and will swim away. This demonstrates that there is no stable configuration of swimmers where they stay close to one another indefinitely.

4.5 Time and size scales in the physical and numerical experiments

In an attempt to relate the physical and numerical units, we recall the physical parameters of bacteria such as *Bacillus subtilis*. The length of the bacterium is around $5\mu\text{m}$ and the typical swimming speed is $\sim 20\mu\text{m}/\text{sec}$. The length of a swimmer in the above numerical experiments is $2a = 0.096$. In these experiments, (40) and (41), the typical forward component of the velocity of a swimmer is

$$0.065 \approx \frac{2 \text{ swimmer body length}}{3 \text{ computer unit of time}}. \quad (43)$$

Since the typical speed of the bacterium is 4 body lengths per second, the unit of computer time for $f_p = 1$ corresponds to

$$(\text{unit of computer time for } f_p = 1) = \frac{2/3}{4} \text{ sec} = 1/6 \text{ sec}. \quad (44)$$

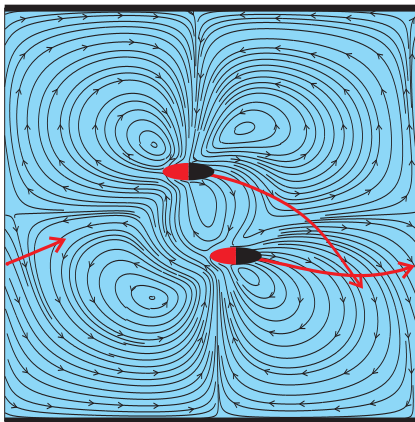


Fig. 6 Figure illustrates the fluid flow for two “offset” parallel microswimmers. Bold red lines show the trajectories each of the swimmers will follow.

Now we compute the physical analogue of the shear rate for the computational experiment with $f_p = 1$. The size of the container is $1/0.096 \approx 10$ lengths of a swimmer, which corresponds to $50\mu\text{m}$. The speed of the top plate relative to the bottom plate is $2 \frac{50\mu\text{m}}{1/6 \text{ sec}} = 600 \frac{\mu\text{m}}{\text{sec}}$. Thus, the shear rate is $\frac{600\mu\text{m}\cdot\text{sec}^{-1}}{50\mu\text{m}} = 12 \text{ sec}^{-1}$.

4.6 Effective viscosity

For a homogeneous fluid, the instantaneous apparent viscosity defined by (20) and the effective viscosity defined by (21) are the same. For an inhomogeneous fluid (e.g., suspensions) (20) takes different values depending on the distribution of inclusions. Figure 7 illustrates sample values of the instantaneous apparent viscosity for a suspension of swimmers as a function of time.

Since in practice the instantaneous apparent viscosity is computed on a finite interval of time it is important to derive an error estimate for the effective viscosity, which is a non-trivial task. Intuitively, the more evaluations one makes (longer simulation time), the more accurate is the estimate of the effective viscosity. However, the same number of samples (time steps) can be done with small or large time step Δt . Small Δt is important for capturing correctly the dynamics of the suspension. Long simulation time is important for the accuracy of the overall estimate of the effective viscosity. Both extremes, million samples with $\Delta t = 10^{-12}$ or hundred samples with $\Delta t = 10$ may be equally poor at predicting the effective viscosity. In the first case, one would get a very accurate dynamics of the suspension, but would miss the range of values. In the second case, one would get a rather broad range of values for completely inaccurate dynamics of the suspension. Since the interaction of swimmers is assumed to play a key role in the effective viscosity the last choice is not satisfactory as well.

We begin by identifying an acceptable time step, which may be a subjective quantity. As a criterion, the time step should be much smaller than the time required to change significantly the instantaneous apparent viscosity. For the propulsion-shear ratio $\frac{f_p}{\mu v} = \lambda$, the appropriate time step was chosen to be $\Delta t_{\text{upper}} = 0.01/\lambda$.

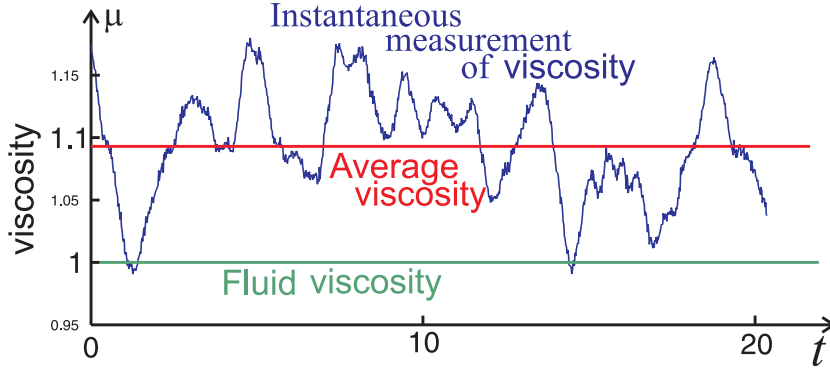


Fig. 7 The green horizontal line indicates the viscosity of the ambient fluid ($\mu = 1$). The blue (oscillating) line shows the instantaneous apparent viscosity as defined by (20). The red horizontal line indicates the time average of the instantaneous apparent viscosity. The computations are performed for the suspension of 25 swimmers at 9% volume fraction in a 1×1 square with periodic boundary conditions in the x -direction. The propulsion of each swimmer is defined by (12) with the total propulsion strength $f_p = 1$ as defined by (13).

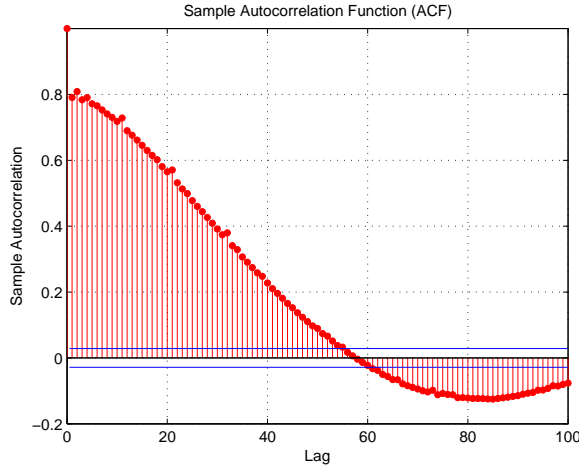


Fig. 8 Autocorrelation function for $f_p = 1$ and time step $\Delta t = 0.02$.

A mean of N independent identically distributed random variables approaches normal distribution with the standard deviation s/\sqrt{N} , where s is the standard deviation of the underlying distribution. In our analysis, all evaluations of the instantaneous apparent viscosity $\bar{\mu}(v; t)$ do not represent independent samples. For example, the correlation between the values of $\bar{\mu}(v; t)$ on two consecutive time steps is more than 0.8 for $\frac{f_p}{\mu v} = 1$. Let n_{lag} be the smallest lag when the autocorrelation equals to zero. As shown in Fig. 8, the zero-autocorrelation lag is $n_{\text{lag}} = 58$ for $\frac{f_p}{\mu v} = 1$. This number indicates that the samples n_{lag} time steps apart are essentially uncorrelated and may be viewed as independent samples.

The total number of time steps divided by n_{lag} is the sample size N . The error in estimating the effective viscosity is then assumed to have a normal distribution with

the standard deviation

$$\frac{\text{standard deviation for the instantaneous apparent viscosity}}{\sqrt{N_{\text{total}}/n_{\text{lag}}}}. \quad (45)$$

The standard deviation of the error, computed according to (45), is shown as vertical error bars on Figure 9.

4.6.1 Effective viscosity as a function of the propulsion-shear ratio

In this section, we analyze the dependence of the effective viscosity on the propulsion-shear ratio $\frac{f_p}{\mu v}$. To compute the effective viscosity, we consider a 1×1 container with periodic boundary conditions on vertical sides and set the shear velocity $v = 1$ on horizontal sides. We fix the size and number of swimmers and vary only their propulsion strength f_p . For each value of f_p , we simulate the dynamics of the swimmers and compute the viscous forces acting on the top and bottom plates and then the instantaneous apparent viscosity as defined by (20).

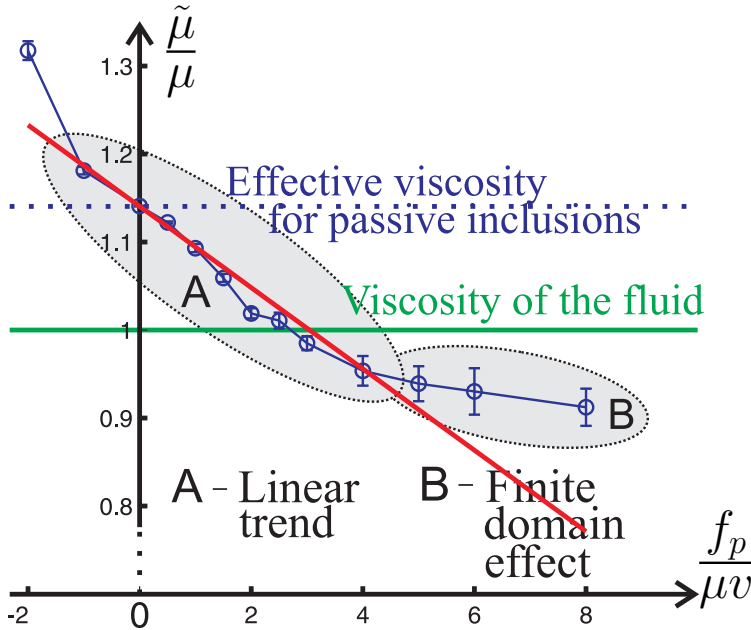


Fig. 9 The points marked by circles indicate the numerically obtained values of the effective viscosity for a given propulsion-shear ratio $\frac{f_p}{\mu v}$. These points are combined into two groups: **A** and **B**. Points in group **A** exhibit linear trend. Points in group **B** exhibit finite domain effects. The solid horizontal line shows the viscosity of the ambient fluid ($\mu = 1$). The dashed horizontal line shows the effective viscosity of a suspension of passive inclusions ($f_p = 0$). The decline straight line shows the weighted least square interpolation to the data.

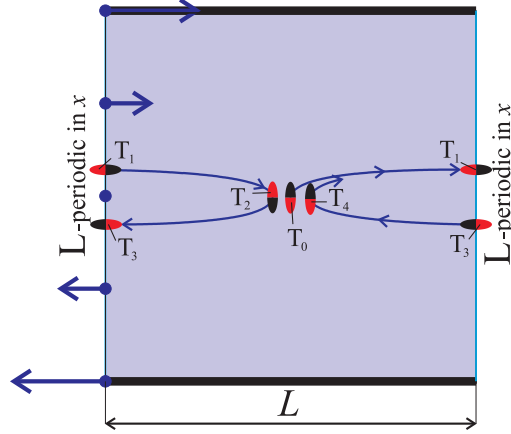


Fig. 10 Sample trajectory of a single swimmer with the propulsion strength $f_p = 1$ in the shear flow $v = 1$. The swimmer's position and orientation at time moments $T_0 = T_4$, T_1 , T_2 , and T_3 are shown.

The effective viscosity as a function of the propulsion strength is shown in Fig. 9. Generally, the standard deviation of the estimates for the effective viscosity is much larger for larger values of the propulsion-shear ratio $\frac{f_p}{\mu v}$. This is due to the fact that the standard deviation of the instantaneous apparent viscosity is proportional to the propulsion strength of the swimmers. Therefore, according to the error estimate (45) to compute the effective viscosity for $\frac{f_p}{\mu v} = 10$ with the same accuracy as for $\frac{f_p}{\mu v} = 1$ it requires not 10 but 10^2 more time steps.

The red line on Figure 9 is given by

$$\alpha \left(\frac{f_p}{\mu v} \right) + \beta, \quad \alpha = -0.046, \quad \beta = 1.141, \quad (46)$$

and represents the weighted least square fit to the data. The weights are inversely proportional to the square of the estimated error in computing each of the data points. Thus, the data points corresponding to larger values of the propulsion-shear ratio and having larger errors effect α and β significantly less than the than data points corresponding to smaller values.

The linear decrease of the effective viscosity is observed for the propulsion-shear ratio ranging from negative one to five. Around $\frac{f_p}{\mu v} \approx 5$ this linear trend is changing. We explain this change by the finite size of the fluid domain. More precisely, we show how the finite size of the container effects the dynamics of a single swimmer. In Fig. 10, we show the trajectory of a single swimmer when the propulsion-shear ratio is one. A single swimmer in a shear background flow swims along an ellipse-like trajectory. The larger is the propulsion-shear ratio, the larger is the vertical semi-axis of this trajectory. For $\frac{f_p}{\mu v} \sim 6$, this semi-axis is half of the container size and no longer fits into the fluid domain. Due to the swimmer-wall interaction, the elliptic-like trajectory of the swimmer deforms significantly at larger values of the propulsion-shear ratio. This explains smooth transition from the linear trend (points in group **A** in Fig. 9) to the finite domain effect (points in group **B**).

Extrapolating the linear trend (46) to the propulsion-shear ratio $\frac{f_p}{\mu v} = 24$, corresponding to the measurements in [3] (shear rate 0.5sec^{-1}), we get an 8.5-fold decrease in the effective viscosity from 1.1408 to 0.1327. This is close to the 7-fold decrease in the viscosity observed in experiments [3].

Heuristically, the decrease of the viscosity due to interactions can be related to the reduction of viscosity in the dilute limit in the presence of the rotational Brownian noise [30]. In this work, it is observed that the rotational Brownian noise breaks up the symmetry (31) in the angular distribution of swimmers and leads to the preferential alignment of swimmers with the shearing flow. Crudely, one can view the interactions between the swimmers as a form of rotational (and translational) noise that has the same effect as the rotational Brownian noise in [30]. The intensity of the rotational noise due to the interactions is proportional to the activity of the swimmers (that is the propulsion strength f_p). The break up of the symmetry (31) and shift of the peaks of the angular distributions of the swimmers can be observed in Fig. 11. The greater is the propulsion strength f_p of the swimmers, the larger is the shift of the peaks in the distributions.

We compared the distribution $p(\theta, f_p)$ of swimmers by angles resulting from hydrodynamic interactions of swimmers with propulsion strength f_p to the distribution $p_{\text{dil}}(\theta, D)$ of swimmers in the dilute limit in the presence of rotational diffusion with coefficient D . The distribution $p_{\text{dil}}(\theta, D)$ solves the Fokker-Plank equation

$$D \frac{\partial^2}{\partial \theta^2} p_{\text{dil}} + \frac{\gamma}{2} \left(1 - \frac{3}{5} \cos(2\theta) \right) \frac{\partial}{\partial \theta} p_{\text{dil}} + \gamma \frac{3}{5} \sin(2\theta) p_{\text{dil}} = 0, \quad (47)$$

where $\gamma = 2$ is the shear rate in the numerical simulations. In both cases, increasing f_p or D leads to the shift in the positive direction of the peak in the distributions $p(\theta, f_p)$ and $p_{\text{dil}}(\theta, D)$, respectively. The distribution $p(\theta, f_p)$ has a more pronounced peak compared with distribution $p_{\text{dil}}(\theta, D)$ and does not flatten as rapidly. The flattening part may be explained by the interactions with the walls.

4.6.2 Distribution of swimmers in the domain

The distribution of swimmers in the domain and their orientations plays a crucial role in determining the instantaneous apparent viscosity.

In physical experiments [31] and some numerical simulations [39,40], it was observed that swimmers tend to aggregate near the walls. In our numerical experiments, we observed this aggregation through computing the time averaged volume density of swimmers as a function of distance from the bottom wall (see Fig. 12). For each horizontal line, we computed the portion of the line covered by swimmers. This number is the instantaneous volume fraction of swimmers and fluctuates with time. To eliminate the fluctuations we take a time average of the instantaneous volume fractions. Due to the top-bottom symmetry of the PDE and random initial conditions, the graph of the distribution is also symmetric.

In [29], it was demonstrated that in the absence of pairwise interactions, shear flow leads to a distribution of swimmers by the angles that decreases the viscosity. In the presence of the pairwise interactions and the swimmer-wall interactions the dynamics of the swimmers is much more complex.

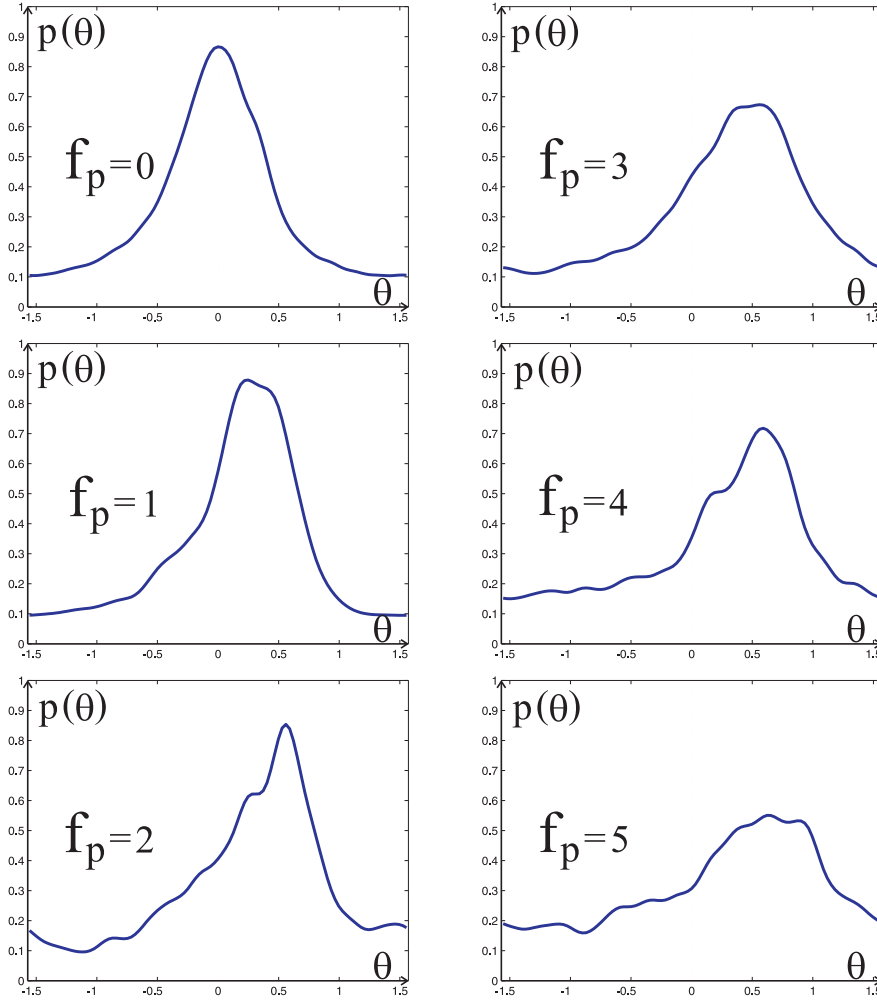


Fig. 11 Distribution of swimmers by angles in the shearing flow ($v = 1$) for different values of the propulsion strength: $f_p = 0, 1, \dots, 5$. The horizontal axis indicates the angle $\theta \in (-\pi/2, \pi/2)$. The vertical axis indicates the distribution density. To remove focus from local irregularities and highlight the global pattern the angular distributions are smoothed by convolution with the Gaussian with mean zero and standard deviation $\pi/40$.

5 Summary

In this work we formulated a well-posed PDE model for the suspension of swimmers which includes the propulsion strength f_p of the swimmers as a parameter. We analyzed the effective shear viscosity of the suspension at the dilute (each swimmer interacts only with the background flow) and moderate concentration regimes.

Using the symmetries of the model, we demonstrated that in the dilute regime the effective shear viscosity of the suspension does not depend on the propulsion strength of swimmers. Hence, in the dilute regime the suspension of active microswimmers has

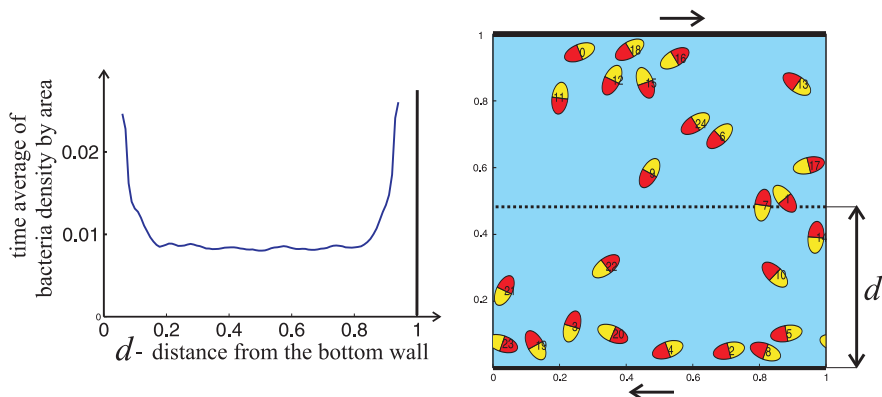


Fig. 12 The right figure shows a sample distribution of 25 swimmers with the propulsion strength $f_p = 1$. The volume fraction of swimmers is 0.09. The left figure shows the time-averaged volume fraction of swimmers as a function of the depth (distance from the bottom wall). Note the increase of the density near the top and bottom walls.

the same effective viscosity as the suspension of passive inclusions of the same shape and at the same concentration. This argument is not specific to our choice of a swimmer and can be applied to a large class of swimmers without any changes. In particular, it can be applied to the swimmers in [21,22,29]. Adding rotational diffusion to the model breaks up the symmetry in the angular distribution of swimmers, leading to preferential alignment of swimmers, which in turn leads to decrease of the effective viscosity for pushers ($f_p > 0$) and increase for pullers ($f_p < 0$).

Using invariance of the PDE model under scaling, we observed the dependence of the effective shear viscosity on the propulsion-shear ratio $\frac{f_p}{\mu v}$ where μ is the fluid viscosity and v is the shear rate of the background flow. This allowed us to analyze the effective viscosity as the function of one parameter.

The numerical simulations performed at the moderate concentrations ($\sim 10\%$ by volume) indicated that the effective shear viscosity decays linearly as a function of the propulsion-shear ratio. This remains true for negative values of the propulsion strength ($f_p < 0$), which corresponds to pullers instead of pushers. We observed the increase of effective shear viscosity for pullers. We found out that the size of the fluid container places an upper bound on the propulsion-shear ratio for which the effective shear viscosity changes linearly. Our numerical experiments indicated that the decrease of the effective viscosity observed in the physical experiments can be explained entirely from a point of view of hydrodynamics. This is an important observation, since biological systems are very complex and include a variety of processes (chemotaxis, oxygen taxis, etc.) that could be hard to isolate in physical experiments. Our mathematical model does not include these phenomena and places the focus only on the hydrodynamic interactions.

Comparison of the results in the dilute and moderate concentration regimes, had shown that changes (increase or decrease) in the effective shear viscosity are not just due to self-propulsion but crucially depend on the swimmer-swimmer interactions. For this reason and as an additional validation of the model and verification of the numerical approach, we performed a number of simulations for two nearby swimmers and for a swimmer next to a wall. The observed results matched with the physically observed

behavior for bacteria. The swimmers attract one another due to lateral suction of fluid induced by self propulsion. But neither two swimmers nor a swimmer next to a wall have a steady state configuration in terms of relative positions.

The method presented in this paper is ideally suited for the complex problems involving swimming microorganisms (e.g. bacteria), where the nature of the experimentally observed phenomenon is not clear a priori. For instance, it may not be clear if the experiment can be explained purely from hydrodynamic considerations or chemotaxis and other phenomena should be considered as well. Our method allows to perform analysis only with hydrodynamic interactions (accurately handling all interactions) and later add chemotaxis if necessary. As an example of physical experiment that could be analyzed by our method we refer to a recent work [33] describing extraction of mechanical energy from “chaotically” swimming bacteria by means of asymmetric gears.

6 Acknowledgements

The work of V. Gyrya and K. Lipnikov was supported in part by the DOE Office of Science Advanced Scientific Computing Research (ASCR) Program in Applied Mathematics Research. The work of V. Gyrya and L. Berlyand was supported in part by DOE grant DE-FG02-08ER25862 and NSF grant DMS-0708324. The work of I. Aranson was supported by the U.S. Department of Energy, Office of Basic Energy Sciences, Division of Materials Science and Engineering, under the Contract number DE AC02-06CH11357.

A Variational formulation and well-posedness of problem (1)-(6)

There are a number of questions that are easier to answer working with the variational formulation of the instantaneous PDE problem (1)-(6). Those questions are the existence and uniqueness of the solution and construction of the appropriate numerical method.

For simplicity of presentation, we derive the variational formulation for a single swimmer. Extension to multiple swimmers is straightforward.

The admissible class of velocity fields, $\mathcal{A}_{\mathbf{g}}$, is the subspace of the Sobolev space $(H^1(\Omega_F))^2$ of vector functions satisfying the boundary conditions (2), (3), and the first one in (4). The linear space of variations, \mathcal{A}_0 , for the admissible class $\mathcal{A}_{\mathbf{g}}$ is obtained by setting $\mathbf{g} = 0$.

Using the second equation in (1), we rewrite the first one as follows:

$$2\mu \operatorname{div} (D(\mathbf{u})) = \nabla p. \quad (48)$$

This is done to obtain symmetrized gradient $D(\mathbf{u})$ and later the stress tensor $\sigma(\mathbf{u}, p)$. Multiplying (48) by $\mathbf{v} \in \mathcal{A}_0$ and integrating by part over Ω_F , we obtain

$$2\mu \int_{\Omega_F} D(\mathbf{u}) : \nabla \mathbf{v} \, d\mathbf{x} - \int_{\Omega_F} p \operatorname{div}(\mathbf{v}) \, d\mathbf{x} = \int_{\partial\Omega_F} \mathbf{n}\sigma(\mathbf{u}, p)\mathbf{v} \, d\mathbf{x}. \quad (49)$$

Let us consider the last integral surface integral in (49). Note that $\partial\Omega_F = \partial\Omega \cup \partial S$, where $\partial S = \Gamma_H \cup \Gamma_P$. Due to the boundary conditions on the test function \mathbf{v} we have that the surface integral over $\partial\Omega$ is zero. The integral over the surface of a microswimmer can be written as

$$\begin{aligned} \int_{\partial S} \mathbf{n}\sigma(\mathbf{u}, p)\mathbf{v} \, d\mathbf{x} &= \int_{\partial S} \mathbf{n}\sigma(\mathbf{u}, p)(\mathbf{v}_C + \omega_{\mathbf{v}} \times (\mathbf{x} - \mathbf{x}_C)) \, d\mathbf{x} \\ &+ \int_{\Gamma_P} \mathbf{n}\sigma(\mathbf{u}, p)\boldsymbol{\tau}((\mathbf{v} - \mathbf{v}_C - \omega_{\mathbf{v}} \times (\mathbf{x} - \mathbf{x}_C)) \cdot \boldsymbol{\tau}) \, d\mathbf{x} \equiv I_1 + I_2. \end{aligned} \quad (50)$$

The balance of forces and torque imply that the first integral is zero:

$$I_1 = \mathbf{v}_C \cdot (\mathbf{F}_H + \mathbf{F}_P) + \omega_{\mathbf{v}} \cdot (\mathbf{T}_H + \mathbf{T}_P) = 0.$$

For the second, integral, we use formula (12) to obtain

$$\begin{aligned} I_2 &= \frac{-f_P}{|\Gamma_P|} (\mathbf{d} \cdot \boldsymbol{\tau}) \left[\int_{\Gamma_P} \mathbf{v} \cdot \boldsymbol{\tau} \, d\mathbf{x} - \int_{\Gamma_P} (\mathbf{v}_C + \omega_{\mathbf{v}} \times (\mathbf{x} - \mathbf{x}_C)) \boldsymbol{\tau} \, d\mathbf{x} \right] \\ &= \frac{-f_P}{|\Gamma_P|} (\mathbf{d} \cdot \boldsymbol{\tau}) \left[\int_{\Gamma_P} \mathbf{v} \cdot \boldsymbol{\tau} \, d\mathbf{x} + \int_{\Gamma_H} \mathbf{v} \cdot \boldsymbol{\tau} \, d\mathbf{x} \right] \equiv L(\mathbf{v}), \end{aligned}$$

which is a linear functional of \mathbf{v} .

Let us introduce the following notations:

$$a(\mathbf{u}, \mathbf{v}) = 2\mu \int_{\Omega_F} D(\mathbf{u}) : \nabla \mathbf{v} \, d\mathbf{x} = 2\mu \int_{\Omega_F} D(\mathbf{u}) : D(\mathbf{v}) \, d\mathbf{x}, \quad (51)$$

$$b(p, \mathbf{v}) = \int_{\Omega_F} p \operatorname{div}(\mathbf{v}) \, d\mathbf{x}. \quad (52)$$

Using these notations, we obtain the variational formulation: Find a pair (\mathbf{u}, p) , $\mathbf{u} \in \mathcal{A}_{\mathbf{g}}$ and $p \in L_0^2(\Omega_F)$, such that

$$\begin{cases} a(\mathbf{u}, \mathbf{v}) - b(p, \mathbf{v}) = L(\mathbf{v}), & \forall \mathbf{v} \in \mathcal{A}_0, \\ b(q, \mathbf{u}) = 0, & \forall q \in L_0^2(\Omega_F). \end{cases} \quad (53)$$

Let $\mathcal{A}_{\mathbf{g}}^{\operatorname{div}}$ be the subspace of $\mathcal{A}_{\mathbf{g}}$ consisting of divergence free functions. Then, a minimization problem, corresponding to the variational problem (53) reads:

$$\min_{\mathbf{u} \in \mathcal{A}_{\mathbf{g}}^{\operatorname{div}}} E[\mathbf{u}], \quad E[\mathbf{u}] = a(\mathbf{u}, \mathbf{u}) - L(\mathbf{u}). \quad (54)$$

The existence and uniqueness of minimizers of (54) is proved by standard arguments provided that the coercivity of the bilinear form $a(\cdot, \cdot)$ can be shown. The coercivity proof, using Korn's inequality, is essentially contained in [41]. In short, for any velocity function with the prescribed trace on a part of the boundary with nonzero two-dimensional measure, we have

$$a(\mathbf{u}, \mathbf{u}) \geq c \|\mathbf{u}\|_1^2, \quad (55)$$

where $\|\cdot\|$ denotes the norm on the Sobolev space $(H^1(\Omega_F))^2$ and constant $c > 0$ depends only on Ω_F .

Finally, the unique field \mathbf{u} that solves (54) is a weak solution of the Stokes equation on a regular bounded domain. By the standard theory (e.g., [42]), there exists a unique pressure field $p \in L_0^2(\Omega_F)$, which together with \mathbf{u} satisfies the a priori L_2 estimates.

References

1. X.-L. Wu and A. Libchaber, "Particle diffusion in a quasi-two-dimensional bacterial bath," *Physical Review Letters*, vol. 84, pp. 3017–3020, March 2000.
2. K. C. Leptos, J. S. Guasto, J. P. Gollub, A. I. Pesci, and R. E. Goldstein, "Dynamics of enhanced tracer diffusion in suspensions of swimming eukaryotic microorganisms," *Phys. Rev. Lett.*, vol. 103, p. 198103, Nov 2009.
3. A. Sokolov and I. S. Aranson, "Reduction of viscosity in suspension of swimming bacteria," *Phys. Rev. Lett.*, vol. 103, p. 148101, Sep 2009.
4. A. Sokolov, R. E. Goldstein, F. I. Feldchtein, and I. S. Aranson, "Enhanced mixing and spatial instability in concentrated bacterial suspensions," *Physical Review E (Statistical, Nonlinear, and Soft Matter Physics)*, vol. 80, no. 3, p. 031903, 2009.
5. A. Einstein, "A new determination of the molecular dimensions," *Annalen der Physik*, vol. 19 (2), pp. 289–306, 1906.

6. G. B. Jeffery, "The motion of ellipsoidal particles immersed in a viscous fluid," *R. Soc. London Ser. A*, vol. 102, pp. 161–79, 1922.
7. L. G. Leal and E. J. Hinch, "The effect of weak brownian rotations on particles in shear flow," *Journal of Fluid Mechanics*, vol. 46, no. 4, pp. 685–703, 1971.
8. L. G. Leal and E. J. Hinch, "The effect of brownian motion on the rheological properties of a suspension of non-spherical particles," *Journal of Fluid Mechanics*, vol. 52, no. 4, pp. 683–712, 1972.
9. G. K. Batchelor and J. T. Green, "The determination of the bulk stress in a suspension of spherical particles to order c^2 ," *Journal of Fluid Mechanics*, vol. 56, pp. 401–427, 1972.
10. T. Levy and E. Sanchez-Palencia, "Suspension of solid particles in a newtonian fluid," *Journal of Fluid Mechanics*, vol. 56, pp. 401–427, 1983.
11. K. C. Nunan and J. B. Keller, "Effective viscosity of periodic suspensions," *J. Fluid Mech.*, vol. 142, pp. 269–287, 1984.
12. L. Berlyand, L. Borcea, and A. Panchenko, "Network approximation for effective viscosity of concentrated suspensions with complex geometry," *SIAM J. Math. Anal.*, vol. 36, no. 5, pp. 1580–1628 (electronic), 2005.
13. L. Berlyand and A. Panchenko, "Strong and weak blow up of the viscous dissipation rates for concentrated suspensions," *Journal of Fluid Mechanics*, vol. 578, pp. 1–34, 2007.
14. L. Berlyand, Y. Gorb, and A. Novikov, "Fictitious fluid approach and anomalous blow-up of the dissipation rate in a 2D model of concentrated suspensions," *Arch. Ration. Mech. Anal.*, vol. 193, no. 3, pp. 585–622, 2009.
15. G. Taylor, "Analysis of the swimming of microscopic organisms," *Proc. Roy. Soc. London. Ser. A.*, vol. 209, pp. 447–461, 1951.
16. E. Purcell, "Life at low Reynolds number," *American Journal of Physics*, vol. 309, no. 45, pp. 3–11, 1977.
17. A. Najafi and R. Golestanian, "Simple swimmer and low reynolds number: Three linked spheres," *Phys. Rev. E*, vol. 69, p. 062901, 2004.
18. R. Golestanian and A. Ajdari, "Mechanical response of a small swimmer driven by conformational transitions," *Physical Review Letters*, vol. 100, p. 038101, 2008.
19. S. Nasserri and N. Phan-Thien, "Hydrodynamic interaction between two nearby swimming micromachines," *Computational Mechanics*, vol. 20, pp. 551–559, 1997.
20. K. Drescher, K. C. Leptos, I. Tuval, T. Ishikawa, T. J. Pedley, and R. E. Goldstein, "Dancing volvox: Hydrodynamic bound states of swimming algae," *Phys. Rev. Lett.*, vol. 102, no. 16, p. 168101, 2009.
21. T. Ishikawa and T. J. Pedley, "The rheology of a semi-dilute suspension of swimming model micro-organisms," *J. Fluid Mech.*, vol. 588, pp. 399–435, 2007.
22. S. Saintillan and M. Shelley, "Orientational order and instabilities in suspensions of self-locomoting rods," *Phys. Rev. Lett.*, vol. 99, pp. 058102:1–4, 2007.
23. A. Sokolov, I. Aranson, J. Kessler, and R. Goldstein, "Concentration dependence of the collective dynamics of swimming bacteria," *Physical Review Letters*, vol. 98, pp. 158102:1–4, 2007.
24. C. Dombrowski, L. Cisneros, S. Chatkaew, R. E. Goldstein, and J. O. Kessler, "Self-concentration and large-scale coherence in bacterial dynamics," *Physical Review Letters*, vol. 93, no. 9, pp. 098103:1–4, 2004.
25. I. Tuval, L. Cisneros, C. Dombrowski, C. W. Wolgemuth, J. O. Kessler, and R. E. Goldstein, "Bacterial swimming and oxygen transport near contact lines," *Proceedings of the National Academy of Sciences*, vol. 102, pp. 2277–2282, 2005.
26. M. E. Cates, S. M. Fielding, D. Marenduzzo, E. Orlandini, and J. M. Yeomans, "Shearing active gels close to the isotropic-nematic transition," *Phys. Rev. Lett.*, vol. 2008, pp. 068102:1–4, 2008.
27. R. Dreyfus, J. Baudry, M. L. Roper, M. Fermigier, H. A. Stone, and J. Bibette, "Microscopic artificial swimmers," *Nature*, vol. 437, no. 7060, pp. 862–865, 2007.
28. Y. Hatwalne, S. Ramaswamy, M. Rao, and R. A. Simha, "Rheology of active-particle suspensions," *Phys. Rev. Lett.*, vol. 92, p. 118101, Mar 2004.
29. B. Haines, I. Aranson, L. Berlyand, and D. Karpeev, "Effective viscosity of dilute bacterial suspensions: A two-dimensional model," *Physical Biology*, vol. 5, pp. 046003:1–9, 2008.
30. B. M. Haines, A. Sokolov, I. S. Aranson, L. Berlyand, and D. A. Karpeev, "Three-dimensional model for the effective viscosity of bacterial suspensions," *Phys. Rev. E*, vol. 80, p. 041922, Oct 2009.
31. A. P. Berke, L. Turner, H. C. Berg, and E. Lauga, "Hydrodynamic attraction of swimming microorganisms by surfaces," *Phys. Rev. Lett.*, vol. 101, p. 038102, 2008.

-
32. M. Short, C. Solari, S. Ganguly, T. Powers, J. Kessler, and R. Goldstein, "Flows driven by flagella of multicellular organisms enhance long-range molecular transport," *Proc. Nat. Acad. Sci. (USA)*, vol. 103, pp. 8315–8319, 2006.
 33. A. Sokolov, M. M. Apodaca, B. A. Grzybowski, and I. S. Aranson, "Swimming bacteria power microscopic gears," *Proceedings of the National Academy of Sciences of The United States of America*, vol. 107, pp. 969–974, January 2010.
 34. V. Gyrya, L. Berlyand, I. Aranson, and D. Karpeev, "A model of hydrodynamic interaction between swimming bacteria," *Bulletin of Mathematical Biology*, vol. 72, pp. 148–183, 2009.
 35. G. K. Batchelor, "The stress system in a suspension of force-free particles," *Journal of Fluid Mechanics*, vol. 41, pp. 545–570, 1970.
 36. L. Beirão da Veiga, V. Gyrya, K. Lipnikov, and G. Manzini, "Mimetic finite difference method for the Stokes problem on polygonal meshes," *J. Comput. Phys.*, vol. 228, no. 19, pp. 7215–7232, 2009.
 37. F. Brezzi, K. Lipnikov, M. Shashkov, and V. Simoncini, "A new discretization methodology for diffusion problems on generalized polyhedral meshes," *Comput. Methods Appl. Mech. Engrg.*, vol. 196, pp. 3682–3692, 2007.
 38. I. S. Aranson and L. S. Tsimring, "Patterns and collective behavior in granular media: Theoretical concepts," *Rev. Mod. Phys.*, vol. 78, pp. 641–692, 2006.
 39. J. Hernandez-Ortiz, C. Stoltz, and M. Graham, "Transport and collective dynamics in suspensions of confined swimming particles," *Physical Review Letters*, vol. 95, pp. 204501:1–4, 2005.
 40. P. T. Underhill, J. P. Hernandez-Ortiz, and M. D. Graham, "Diffusion and spatial correlations in suspensions of swimming particles," *Phys. Rev. Lett.*, vol. 100, pp. 248101–1–4, 2008.
 41. G. Duvaut and J. L. Lions, *Inequalities in Mechanics and Physics*. Springer, 1976.
 42. G. P. Galdi, *An introduction to the mathematical theory of the Navier-Stokes equations. Vol. I*, vol. 38 of *Springer Tracts in Natural Philosophy*. New York: Springer-Verlag, 1994. Linearized steady problems.